Multi-GHz Monitoring of Cement Hydration using Time Domain Reflectometry Dielectric Spectroscopy

N. E. Hager III,[1,2] R.C. Domszy,[1,2] and M. R. Tofighi[3]

[1]Dept of Physics and Engineering, Elizabethtown College, Elizabethtown, PA, 17022, USA
[2]Material Sensing & Instrumentation, Inc., 772 Dorsea Rd. Lancaster, PA 17601, USA
[3]Electrical Engineering, The Pennsylvania State University at Harrisburg, Middletown, PA, 17057, USA

The compressive strength of concrete is directly related to the degree of hydration in the cement paste. Our prior work demonstrated a continuous monitoring of the physical state of water in hydrating cement paste from around 10 kHz to several GHz throughout the cure process. The broadband complex permittivity was monitored as a function of cure time using Time-Domain-Reflectometry (TDR) Dielectric Spectroscopy and an embedded capacitance sensor. Current work now focuses on extending the frequency range to around 12-15 GHz, to more fully capture the free-water relaxation occurring in this range and separate it from the bound-water relaxation occurring at lower frequencies. New methods being developed include a TDR Smith chart, which displays the TDR transient in a complex reflection-coefficient plane, accentuating differences between expected sensor loading and unwanted signal artifacts. Such artifacts may include reflections from sample boundaries, resonance in the sensing pin, reflections from shielding arrangements, and errors in numerical transforms. Other methods include improved calibration using reference liquids which closely match the real and imaginary permittivity of hydrating cement at various stages of cure. In fresh cement paste, where water-loading and ion conductivity is high, a mixture of saline and Poly(methyl methacrylate) (PMMA) powder provides a reference with a relaxation time similar to pure water, but at a reduced permittivity and increased conductivity comparable to fresh cement paste. At longer cure times, where water-loading and ion conductivity are minimal, references such as tetrahydrofuran with added electrolyte provide a comparable relaxation reference and reduced conductivity comparable to cured paste. These two references set a high and low "calibration window" through which the real and imaginary permittivity can be monitored over a wide range in cure. To verify dispersion in the captured TDR transient directly, transients are compared in the time domain with constant-permittivity references to ensure expected stretched exponential behavior is present. Methods should have broad applications in a variety of inorganic/organic materials and aqueous systems of interest in groundwater characterization.

Introduction

The setting of ordinary portland cement (OPC) is caused by the formation of calcium silicate hydrate (C-S-H)[1] by a dissolution-precipitation process[2] that occurs when calcium silicates react with water. The ultimate properties of concrete such as compressive strength and pore structure are governed by these hydration reactions, and hence the service life of concrete is largely controlled by cure conditions.

Techniques to characterize the nature of the water reactions include Nuclear Magnetic Resonance (NMR) relaxation measurements,[3,2] solid-state ^{1}H NMR experiments[4] and quasi-elastic neutron scattering (QENS).[5,6] A variety of electrical methods can also be used including low frequency methods, which follow dissolved alkali ions in percolative channels, and high-frequency methods, which monitor the ability of the water molecule to reorient in an applied electric field. Pervious work in our laboratory[7] demonstrated a Time Domain Reflectometry (TDR) method for monitoring of the dielectric relaxation spectrum in hydrating cement paste, over the frequency range 10 kHz to several GHz from initial mixing to several weeks cure.

A limitation has been obtaining reliable information over 10 GHz where the free-water relaxation occurs.[8] Information in this range is desirable, as it more clearly separates the free-water relaxation occurring around 18 GHz from the bound-water relaxation occurring below 1 GHz. We have recently developed a TDR Smith chart technique[9] to isolate small instrument artifacts captured in the reflected signal from dielectric response, which become accentuated by Laplace transform and differential methods used in processing and calibration. The focus here is to apply this and other calibration methods to obtain complex permittivity spectra in cement paste to around 15 GHz, continuously as a function of cure time.

Background[9]

The expressions governing TDR Dielectric Spectroscopy are described in the literature.[10] An incident voltage pulse $v_i(t)$ propagating along a transmission line of characteristic admittance G_c encounters a terminating capacitive sensor of admittance Y producing a reflected pulse $v_r(t)$. The terminating admittance is the total current-to-voltage ratio $G_c(v_i - v_r)/(v_i + v_r)$, where v_i and v_r are the Laplace transforms of the incident and reflected pulses. The terminating admittance is related to sample permittivity ε by $Y = i\omega\varepsilon C_o$, so the permittivity is written as:

$$\varepsilon(\omega) = \frac{G_c}{i\omega C_o}\frac{v_i - v_r}{v_i + v_r} \qquad \textbf{Equation 1}$$

where C_o is the geometric capacitance of the open terminated sensor.

To establish a common time reference, the incident voltage is substituted by the empty sensor reflection, by writing Equation 1 for both empty sensor and sample reflections and manipulating the two equations to eliminate v_i. The result is a relative *reflection function* $\rho(\omega)$[10] of similar form:

$$\rho(\omega) = \frac{G_c}{i\omega C_o}\frac{v_{r,r} - v_{r,x}}{v_{r,r} + v_{r,x}} \qquad \textbf{Equation 2}$$

where $v_{r,r}$ and $v_{r,x}$ are the reflected pulse's Laplace transforms for the empty sensor and sample reflections. Alternatively, the reflection function $\rho(\omega)$ can be written in terms of a relative *reflection coefficient* Γ_{rel}

$$\rho(\omega) = \frac{G_c}{i\omega C_o}\frac{1 - \Gamma_{rel}}{1 + \Gamma_{rel}} \qquad \textbf{Equation 3}$$

where $\Gamma_{rel} = v_{r,x}/v_{r,r}$ is the *reflection coefficient*[9] of the unknown signal relative to the empty-sensor signal.

The complex permittivity is then obtained from a differential expression:

$$\varepsilon(\omega) = \frac{\rho + 1}{1 - (\omega C_o/G_c)^2\rho} \qquad \textbf{Equation 4}$$

where the denominator represents the offset between the incident pulse and the empty sensor reflection at the measurement plane. The complex permittivity can also be written in bilinear form, to remove transmission line effects:

$$\varepsilon = \frac{(1 + A)\rho + C}{1 - B\rho} \qquad \textbf{Equation 5}$$

where complex parameters A, B, and C are determined using calibration with known reference standards. [9]

A key step is displaying the initially transformed data in the complex plane as a relative reflection coefficient, thus providing a simple Smith chart as a diagnostic for unwanted signal artifacts. The relative reflection coefficient approximates the absolute reflection coefficient $\Gamma_x = v_{r,x}/v_i$, provided the empty-sensor capacitance is small and empty-sensor reflection approximates the incident pulse. Real and imaginary components are plotted on the lower capacitive half of the Smith chart as a function of frequency, with the approximate sensor admittance read from the susceptance and conductance circles. Since Γ_{rel} is referenced to the empty-sensor, reflection losses in the transmission line do not appear, and losses appearing on the Smith chart are

due to sample losses. An increasing real permittivity produces an increasing sensor susceptance, following a path around the lower perimeter of the Smith chart, while an increasing sample loss produces an increasing sensor conductance, following a path which spirals inward on the Smith chart. Artifacts in acquisition or Laplace transform appear as deviations from this expected behavior; these may include resonance of the sensing pin, reflections within the sample boundaries, resonance of the sensing pin, or improper Laplace transform settings. The TDR Smith chart thus provides a quick method for assessing sensor response and material characteristics in the multi-GHz range, which requires no calibration and is only one computational step removed from the direct TDR transient.

Procedures

Measurements are made in Portland cement paste mixed in a water-to-cement ratio of 0.35. The fresh paste is placed in a styrofoam cup with the sensor immersed and cup sealed to prevent evaporation. The sensor is a 20-30 cm length of 3.5 mm semi-rigid coaxial line (MicroCoax UT-141) in which one end is ground mechanically flat. This provides a terminating capacitance of around 20 fF into the sample material, as determined by calculating the reflection function ρ (Equation 3) matching to a known permittivity in the low-frequency limit, and working backwards to obtain the sensor capacitance C_o.

Calibration liquids are chosen to tightly straddle the range of permittivity and frequency response expected during cement cure. We assume the fresh cement paste contains a strong water-like relaxation, reduced in amplitude by the water/solids ratio.[11,12] We make no assumption for the cured cement, and choose a low-permittivity calibration which varies only slowly with frequency in permittivity and loss.

For the fresh cement paste, a mixture of saline and PMMA beads (Acros Organics, m.w. 35,000, diam. 50-150 μm) provides an 8.2 ps water-like relaxation at the reduced permittivity ($\varepsilon' \approx 40$) and water/solids ratio of fresh cement paste. The bulk PMMA relaxation is negligible[13], and the saline has a conductivity that matches the cement conductivity. To ensure uniformity, the mixture is stirred with a magnetic stirrer during measurement. At longer stages of cure, a low-permittivity solvent with a very high relaxation frequency provides a slowly deceasing real permittivity $\varepsilon'(\omega)$ and a slowly increasing imaginary permittivity $\varepsilon''(\omega)$ through the range. Solvents such as tetrahydrofuran[14] (THF) or dichloromethane[15] work appropriately, with a small amount of electrolyte added[16,17] to increase low frequency conductivity. A finite conductivity is needed to keep calibration

and empty-sensor signals resolvable from one another, so bilinear parameters can be generated over the entire frequency range.

Signals are acquired with an Agilent 54750 TDR oscilloscope with a 54754A differential plug-in, which has a 35-ps internal voltage step and a 20-GHz detection bandwidth. Reflected signals are captured non-uniformly on consecutive linear time segments[18], starting at 10 ps/cm and increasing to 500 μs/cm in an automated sequence. At the beginning of the sequence the incident pulse is captured and used as a timing reference, with a feedback algorithm adjusting the timing of all later segments to provide drift control. Small jitter between segments is further minimized by scanning the entire sequence repetitively and averaging, thus minimizing jitter between the incident and initial reflected pulses during sequencing. The incident and initial reflected pulses are captured at 2000 points to provide a timing resolution of 50 fs/point, with later segments gradually reduced to 200 points per segment. Other settings are typically 12 time segments, with 32x signal averaging for each segment, and 8 repetitions of the entire sequence for a total acquisition time of 3-4 minutes. Since the scope is AC-coupled, a vertical correction is applied to each segment to remove DC offsets from electrochemical effects and splice it smoothly with the preceding segment.

To reduce excessive computation and noise the linear segmented data is interpolated onto a logarithmic time scale prior to Laplace transform, using cubic-spline algorithms found in most math software. Each segment is first run through a median smoothing filter to minimize noise and provide additional signal averaging. Then the smoothed data is interpolated linearly up to the peak of the reflected transient, and logarithmically for all times thereafter. The linear interpolation is spaced at 5 ps per point, consistent with a 100 GHz Nyquist sampling frequency which is well above the 20 GHz bandwidth of the scope. The logarithmic interpolation starts at 5 ps per point and increases at a rate of around 50-60 points per decade.[19] A numerical Laplace integration is performed over the interpolated data with the integration interval adjusted to the logarithmic data spacing. Further details are found in the references.[9]

Results

Reflected transients are shown in Figure 1 for saline/PMMA high calibration, a THF/zinc nitrate low calibration, and hydrating cement paste at cure times of 0 h, 8 h, 24 h, and 72 h. In each case segment 1 is the timing reference, segment 2 is the initial reflected transient, and segments 3-12 are the continuation of the initial

reflected transient on increasing time scales. The empty sensor returns a positive reflection indicating the open-circuit reference, while the liquids return an increasing negative reflection whose exponential decay is governed by the loaded sensor capacitance and the 50 Ω (0.02 S) line impedance. The negative peak reflection amplitude decreases with increasing permittivity, and the stretched-exponential decay follows the changing permittivity and loss with frequency. In TDR measurements of calibration samples and cement paste, the stretched-exponential decay spans many decades due to ionic conduction and electrode polarization. The high calibration uses approximately 0.5 M saline in PMMA, and the low calibration uses approximately 0.4 M ($Zn(NO_3)_2 \cdot 6H_2O$) in THF.

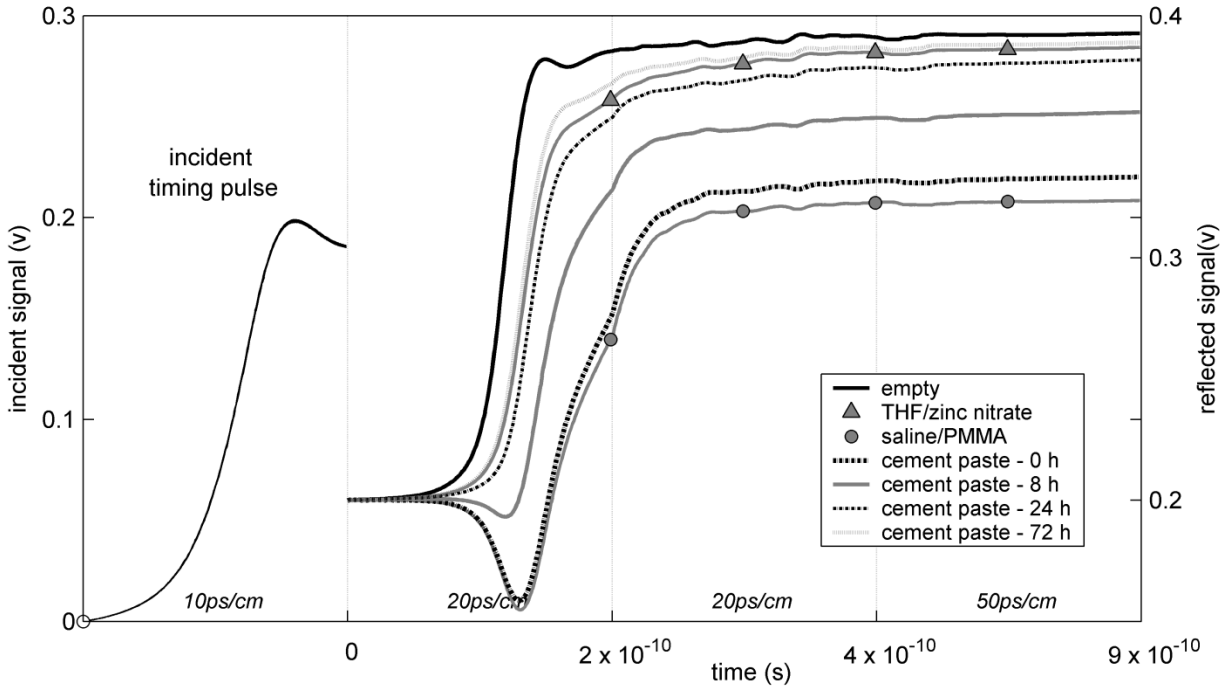

Figure 1 - Segmented transient acquisition for calibration liquids and cement paste with 3.5-mm flat termination (4 of 12 segments shown).

The corresponding Smith charts for the reflected transients are shown in Figure 2. The figure uses an admittance Smith chart, with susceptance/conductance circles originating from the left, displaying the terminating admittance (proportional to permittivity) in the standard manner as a parallel combination of capacitance and conductance. Circles of constant susceptance and constant conductance are labeled, normalized to the 0.02 S (50 Ω) line admittance. For each transient, the Smith chart shows the load susceptance $\varepsilon'\omega C_o$ increasing with frequency, crossing lines of constant susceptance and tracing an arc around the lower perimeter

of the chart. Selected frequency points are labeled, starting at 2 GHz on the right and continuing to 16 GHz on the left.

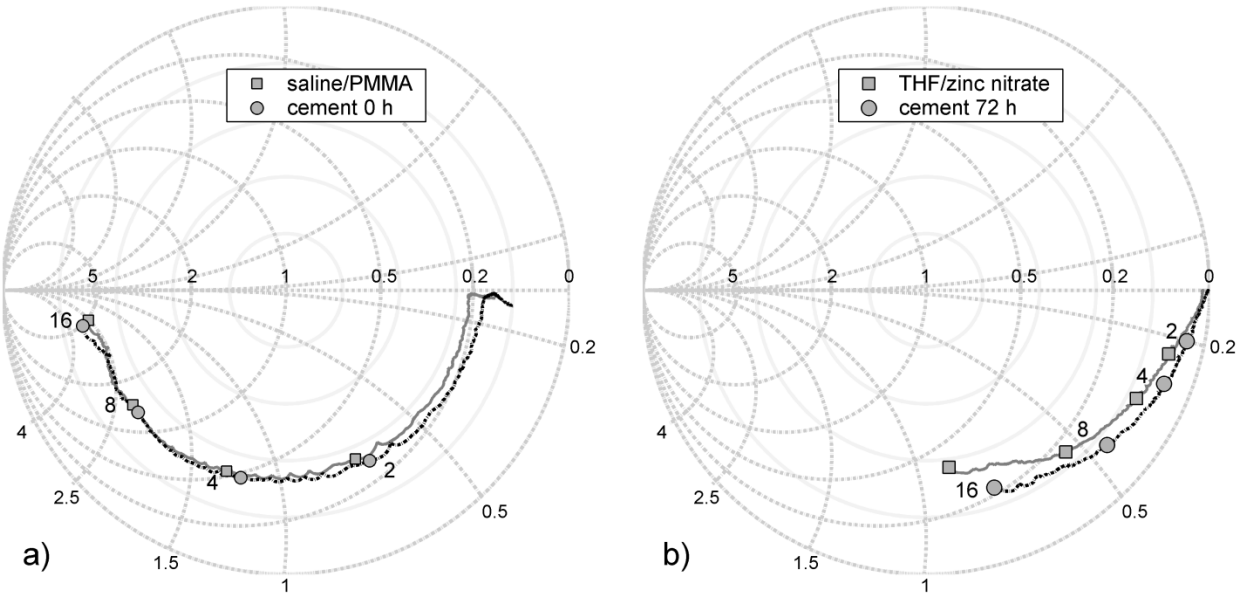

Figure 2 - TDR Smith charts for calibration liquids and cement paste at 0 h and 72 h cure. Frequency markers are shown in GHz.

Figure 2 shows the relative reflection coefficient Γ_{rel} for two different cure levels. Figure 2a shows the fresh cement paste signal at 0 h compared with the saline/PMMA reference. The two signals follow a smooth circle around the lower interior of the complex plane, showing a rapid increase in susceptance with frequency and following a circle of constant conductance. No large deviations due to sample boundary reflections[9] or Laplace transform artifacts are seen. The susceptance approaches resonance at around 16 GHz (negative real axis) where the absolute reflection coefficient Γ_x crosses into the inductive region.[9] Fig 2b shows the cement signal at 72 h compared with the THF/zinc nitrate reference. The permittivity is now reduced at the lower free-water loading, and Γ_{rel} traces a shorter path around the lower perimeter of the diagram. The conductivity has also decreased, as Γ_{rel} at low frequencies moves to the outer perimeter of the diagram. Γ_{rel} spirals inward with increasing frequency, indicating an increasing loss factor $\varepsilon''(\omega)$. The Smith chart thus provides a quick way showing the data is behaving as expected and is free of unwanted artifacts, before proceeding to the next step of calibration.

Figure 3 shows the reflection function $\rho(\omega)$ for the 2 calibration liquids. Real and imaginary parts are shown as a function of frequency, and overlaid with dielectric models for the expected behavior for both calibrations. ρ'' is multiplied by $\varepsilon_0\omega$ to display the conductivity, thus removing the ω^{-1} dependence at low

frequencies and displaying as a deviation from constant conductivity (displayed on a log scale). For the THF/zinc nitrate calibration, the model includes a 4 ps solvent relaxation (Debye), a 200 ps solute relaxation (Cole- Davidson β= 0.8), a solvent relaxation magnitude of 8, a solute relaxation magnitude of 9, and a 0.11 S/m ion conductivity. For the saline/PMMA calibration, the model includes an 8.2 ps free-water relaxation (Debye), an adjustable free-water relaxation magnitude, and a 1.9 S/m ion conductivity. Complex bilinear parameters $A(\omega)$ and $B(\omega)$ are generated by solving Equation 5 for 2 calibration references, and separating real and imaginary parts into 4 simultaneous equations. Details are given in the references.[9]

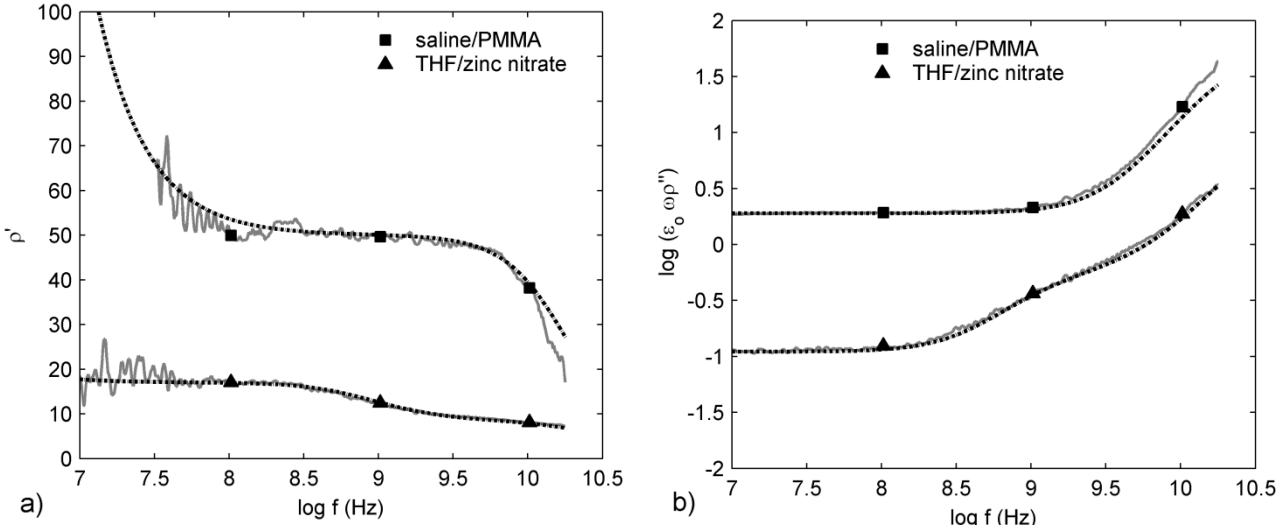

Figure 3 – Reflection function ρ' and $\varepsilon_o\omega\rho''$ for calibration liquids and model fit for THF/zinc nitrate and saline/PMMA.

Figure 4 shows the calibrated cement permittivity for the data in Figure 1, calibrated using the bilinear parameters obtained from Figure 3. The data is valid to around 15 GHz, and shows that at around 10 GHz the permittivity ε' starts decreasing and the conductivity $\varepsilon_o\omega\varepsilon''$ starts increasing. As cure proceeds both the magnitude ε' over the range decreases as well as the magnitude of the 10 GHz transition. Simultaneously, the magnitude of the conductivity $\varepsilon_o\omega\varepsilon''$ (displayed on a log scale) decreases over the range as well as the magnitude of the 10 GHz peak transition. A broad feature appears around 100 -1000 MHz in the conductivity, which should be due to the bound water signal observed previously.[7]

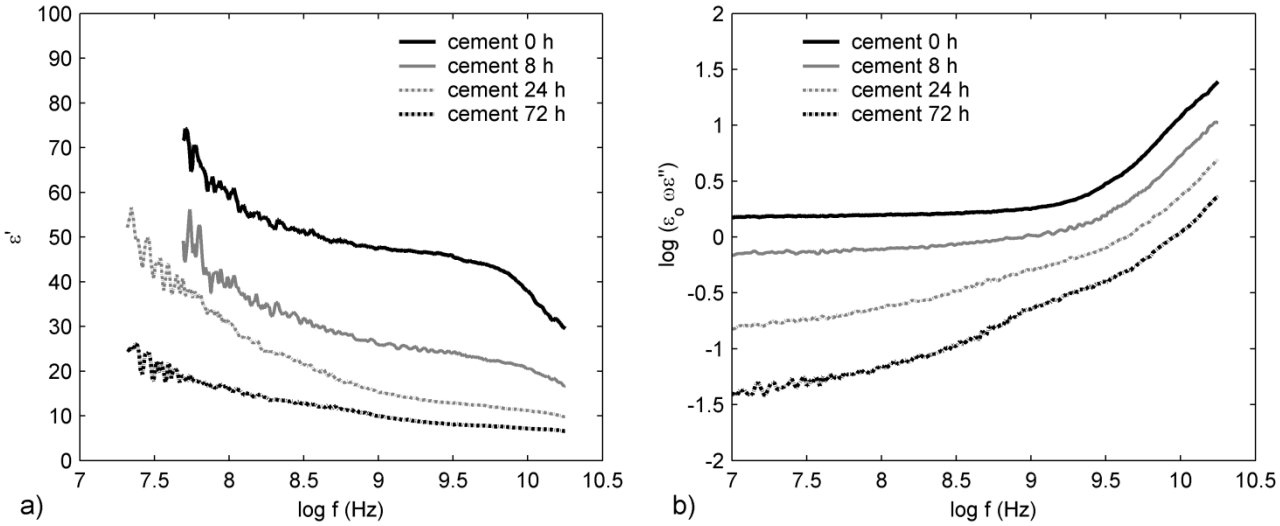

Figure 4 – Calibrated real permittivity ε' and conductivity $\varepsilon_o\omega\varepsilon''$ during cement cure.

The entire signal evolution remains within the calibration "window" defined in Figure 3 for both real and imaginary components. The relaxation amplitude decreases in both permittivity and conductivity as cure proceeds, as water is consumed in reaction. Sensitivity is gained in the 10-15 GHz range, critical to resolving free-water behavior, but lost below 100 MHz due to the lower sensor capacitance. (20 fF). It would seem reasonable that data could be captured over the entire range 10 kHz to 15 GHz, using the current sensor with a flat termination (20 fF) and the previous sensor with protruding pin[7] (100 fF) running in tandem.

Discussion

We have demonstrated the monitoring of complex permittivity of hydrating cement paste in the 100 MHz to 15 GHz range continuously as a function of cure time. This bandwidth is sufficient to observe details of 18 GHz free-water relaxation, and separate it from the bound-water relaxation occurring below 1 GHz. This bandwidth is achieved through the use of Smith chart analysis, to control small unwanted artifacts, and the use of calibration standards which tightly define a calibration "window" for the range of frequency and cure state.

Future work should include a low-calibration model system with a similar permittivity and conductivity, but with a lower or negligible solute relaxation. A candidate for this could be dichloromethane with perchlorate salts.[15,16] Additional work will involve using a complex model fit[7] to fully separate free- and bound-water components as a function of cure time. Additional components would be included in the model, such as a limiting high-frequency permittivity ε_∞ to better fit the $\varepsilon'(\omega)$ roll-off.

Acknowledgement

This work was supported in part by the National Science Foundation under grant number 0700699.

[1] Cement chemistry notation: C = CaO, S = SiO_2, H = H_2O, A = Al_2O3.

[2] H. F. W. Taylor, Cement Chemistry, 2nd ed. (Thomas Telford Publishing, London, 1997).

[3] R. J. Wittebort, M. G. Usha, D. J. Ruben, D. E. Wemmer, and A. J Pines, J. Am. Chem. Soc, **110**, 5668 (1988).

[4] R. Rassem, H. Zannitheveneau, D. Heidemann, and A. Grimmer, Cement and Concrete Research, **23**, 169- (1993)

[5] S. A. FitzGerald, D. A. Neumann, J. J. Rush, D. P. Bentz, and R. A. Livingston, Chem. Mater. **10**, 397 (1998).

[6] J. J. Thomas, S. A. FitzGerald, D. A. Neumann, and Richard A. Livingston, J. Am. Ceram. Soc. **84** (8), 1811 (2001).

[7] N. E. Hager III and R. C. Domszy, J. Appl. Phys. **96**, 5117-5128 (2004).

[8] U. Kaatze, J. Molecular Liquids, **56**, 95 (1993).

[9] N.E. Hager III, R.C. Domszy, M.R. Tofighi, Rev. Sci. Instrum. 83, 025108 (2012).

[10] R. H. Cole, J. G. Berberian, S. Mashimo, G. Chryssikos, A. Burns, E. Tombari, J. Appl. Phys. **66**, 793 (1989).

[11] D.A. Robinson, S.P. Friedman, J. Non-Crystalline Solids 305, 261 (2002).

[12] S. B. Jones, S. P. Friedman, Water Resources Research, 36 (10), 2821c (Oct 2000).

[13] S. Mashimo, H. Nakamura, A. Chiba, J. Chem. Phys, 76, 6342 (1982).

[14] A. C. Khumbharkhane, et al, Pramana J. Phys., Vol. **46** (2), 91 (Feb 1996).

[15] J. Hunger, A. Stoppa, A.Thoman, M. Walther, R. Buchner, Chem. Phys. Lett. **471**, 85 (2009).

[16] B. Gestblom, J. Songstad, Acta Chemica Scandinavica, **B41**, 396 (1987).

[17] H. Farber, J. Petrucci, J. Phys. Chem., **79(**12) 1221 (1975).

[18] N.E. Hager III, Rev. Sci. Instrum. **65**, 887 (1994).

[19] F. I. Mopsik, Rev. Sci. Instrum. **55**, 79 (1985).